Journal of Nanotechnology & Advanced Materials
An International Journal

http://dx.doi.org/10.18576/jnam/050104

Preparation, Chiroptical and Photoluminescence Studies of Size Selected Gold Nanoclusters

Mostafa Farrag[*]

Chemistry Department, Faculty of Science, Assiut University, 71516 Assiut, Egypt.

Received: 5 Apr. 2016, Revised: 20 Oct. 2016, Accepted: 22 Oct. 2016.
Published online: 1 Jan. 2017.

Abstract: Here, we used the methanol-induced precipitation method to prepare and separate two size selected gold clusters protected by two enantiomers and racemic mixture of penicillamine ligand. The clusters materials were obtained by the reduction of $HAuCl_4 \cdot 3H_2O$ salt with $NaBH_4$ in the presence of L-penicillamine (L-pen), D-penicillamine (D-pen) and racemic mixture of penicillamine (rac-pen) as capping ligands. Two fractions were obtained with particles of about 1 nm and 2.6 nm, respectively. The average chemical formula was determined from thermogravimetric analysis (TGA). The optical properties of the samples were studied by three different methods: UV-vis spectroscopy, photoluminescence spectroscopy (PL) and circular dichroism (CD) spectroscopy. PL studies yielded the fluorescent properties of the samples. The main focus of this work, however, lies in the chirality of the particles. The CD spectra for gold clusters capped with one of the two enantiomers (D- or L-form) typical CD spectra were observed, no significant signals were detected for a racemic ligand mixture. Furthermore, gold clusters show quite large asymmetry factors (up to $1.3x10^{-3}$) in comparison to most other ligand protected clusters. These large factors and bands in the visible range of the spectrum suggest a strong chiral induction from the ligand to the metal core.

Keywords: Size selected gold clusters; Chirality; Photoluminescence Spectroscopy; Methanol-induced method; L/D-Penicillamine

1 Introduction

Gold nanoclusters protected by ligands, such as thiolates [1–5], phosphines [6,7] and amines [8,9], have attracted great interest since they are promising materials for both fundamental research and applications. The structure, bonding and stability of the thiolate-protected Au clusters are being intensely pursued [1–5]. A series of size selected gold cluster protected by different ligands (SR) were separated such as Au_{25}, Au_{38}, Au_{68}, Au_{102} and Au_{144} [1–5]. Single crystal X-ray diffraction was used to determine the crystal structure of these size selected gold clusters [1,10,11]. In addition, $Au_{25}(SR)_{18}$ exhibits many interesting properties that are not observed in bulk gold, such as photoluminescence [2] and paramagnetism [12].

Whereas the general properties such as the optical spectrum, electronic structure of size selected clusters are well-understood, their chiroptical properties are barely studied. Several examples of chiral gold nanoclusters have been presented in the past [13,14] and conformational analysis of the adsorbed ligand was performed using vibrational circular dichroism [15,16]. Moreover, the crystal structures of $Au_{38}(SR)_{24}$ and $Au_{102}(SR)_{44}$ bear intrinsic chirality [1,17]. Since the discovery of optical activity in glutathionate protected clusters [2,13], a series of ligands was examined; mostly cysteine-derivatives [13,15,18]. Due to lack of methodology, synthesis and characterization of monodisperse chiral gold clusters is rare. Recently, major breakthroughs were size-conserving ligand exchange experiments [19,20] and successful synthesis of chiral $Au_{25}(SR)_{18}$ [21]. This cluster bears a Au_{13} core covered by six long staples (SR-Au-SR-Au-SR) [22]. The core and the arrangement of the staples on the latter are not chiral, in contrast for example to $Au_{38}(SR)_{24}$. Therefore, the observed optical activity has to be linked to the chirality of the adsorbed thiolates (SR) [17,23]. Two enantiomers of gold clusters protected by the achiral 2-phenylethanethiol ligands ($Au_{38}(SCH_2CH_2Ph)_{24}$) and ($Au_{40}(SCH_2CH_2Ph)_{24}$) were separated by chiral high-performance liquid chromatography (chiral HPLC) [23]. The enantiomers show mirror-image circular dichroism responses and large anisotropy factors of up to $4x10^{-3}$ and $6x10^{-3}$, respectively [23].

[*]Corresponding author e-mail: mostafafarrag@aun.edu.eg

In this study, we used methanol-induced precipitation method [2] to synthesize gold clusters protected by chiral L- and D-penicillamine (scheme 1) as well as their racemic mixture (rac-pen). Gold clusters protected by the same ligands were synthesized by another synthesis method [18], clusters with a rather large size distribution were obtained and subsequently subjected to gel electrophoresis for obtaining fractions of different cluster sizes. While such an approach produces very limited yield due to the separation by gel electrophoresis. The method used in this work, however, is purely based on wet chemistry and has the advantage of a strongly increased yield of the cluster material. The particle size and their average chemical formula for synthesized clusters were assessed by transmission electron microscopy (TEM) and thermogravimetric analysis (TGA), respectively. Furthermore, it is found that the optical properties of the clusters in this work differ from those previously reported ones. We attribute this to different cluster morphology, which indicates that different types of clusters are obtained by our preparation technique. The optical properties of enantioselective gold clusters were studied by circular dichroism (CD) and photoluminescence spectroscopy (PL). In the following we present the cluster synthesis and the characterization of the samples by electron microscopy, thermogravimetric analysis and optical spectroscopy.

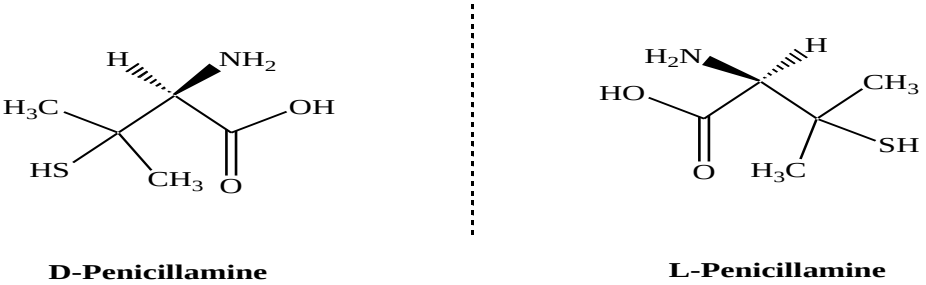

D-Penicillamine **L-Penicillamine**

Scheme 1: L- and D- penicillamine (L- and D-pen) used as ligands for protecting the clusters.

2 Experimental

In this work several gold cluster samples were isolated and studied. Gold clusters were obtained with different enantiomers of the ligand and subsequently subjected to methanol induced precipitation. This precipitation method resulted of two different sizes gold clusters, small clusters of about 1 nm and larger clusters comprising of an average of 4 nm cores.

2.1 Chemicals

Tetrachloroauric (III) acid ($HAuCl_4 \cdot 3H_2O$, >99.99% metals basis, Aldrich), Sodium borohydride ($NaBH_4$, ≥96%, Aldrich), L-penicillamine (L-pen, 99%, Aldrich), and D-penicillamine (D-pen, ≥99%, Sigma-Aldrich) were used in the synthesis of the ligand protected gold nanoparticles (for the chemical structure of D- and L-pen see scheme 1). As solvents ethanol (HPLC grade, Aldrich) and methanol (HPLC grade, Aldrich) were taken. All chemicals were used as received. All glassware was thoroughly cleaned with aqua regia ($HCl:HNO_3$ = 3:1 v/v), rinsed with distilled water, and then dried in an oven prior to use.

2.2 Preparation of $Au_n(L\text{-}pen)_m$, $Au_n(D\text{-}pen)_m$ and $Au_n(rac\text{-}pen)_m$ Nanoclusters

Tetrachloroauric (III) acid (104 mg, 0.264 mmol) was first dissolved in 2nd distilled water (30 ml) in a round flask. The solution was then cooled to around 0°C with an ice bath over a period of 30 min. Afterwards, L-penicillamine (L-pen) or D-penicillamine (D-pen) or racemic mixture of penicillamine (rac-pen) ligands (157 mg, 1.06 mmol) were slowly added to the flask under slow magnetic stirring (~60 rpm). The solution was then stirred for 1.5 h. Subsequently, $NaBH_4$ (100 mg, dissolved in 15 mL ice-cold water) was rapidly added to the clear gold salt solution under vigorous stirring (~1200 rpm). The solution immediately became dark, indicating the reduction of the gold salt and the formation of nanoparticles. The reaction was allowed to proceed for another 12 h. Then, MeOH (40 mL) was slowly added under constant stirring. Subsequently, the precipitates (fraction 1) were collected by centrifugation (5000 rpm, 10 min), washed with methanol three times and then dried under reduced pressure. After concentrating, the remaining supernatant fraction 2 was isolated by adding more MeOH. The precipitate was washed with MeOH and then dried by vacuum filtration.

2.3 Instrumentation and Characterization

To obtain the UV−vis absorption spectra of the prepared nanoclusters, aqueous solutions of approximately 1 mg/ml were prepared. The spectra were recorded at ambient temperature from 200 to 900 nm with a double-beam spectrophotometer (Evolution 300). The CD spectra of all types of clusters were measured with a Jasco J-710 spectropolarimeter, using a

quartz cell of 1 cm path length and solutions with the same solvent and concentration as for UV−vis spectroscopy. Thermal gravimetric analysis (TGA, ~ 2 mg sample tested) was conducted in a N_2 atmosphere (flow rate ~50 ml/min) with a ThermoStartTM TG/DAT (Pfeiffer Vacuum). All measurements were performed with a heating rate of 10°C/min, starting from room temperature and ramping up to 900°C. For TEM measurements, solutions with a concentration of 1−2 mg/mL were prepared by dissolving or suspension the catalysts materials in 2nd distilled water. A droplet of these catalysts solutions was casted onto carbon-coated copper grids. The solvent was then allowed to evaporate slowly. TEM images were obtained at a magnification of 200,000 and 120,000 for fraction 1 and fraction 2 gold clusters, respectively, with a high resolution transmission electron microscope (HRTEM) TECNAI G^2 spirit TWIN at acceleration voltage of 120 kV, conducted by VELETA Camera. The images were then analyzed by using Image J software (version 1.44). Photoexcitation and fluorescence studies were performed with a JASCo FP-6300 spectrofluorometer with a xenon lamp as excitation source. The band-pass for both, excitation and emission monochromators, was always kept at 5 nm.

3 Results and Discussion

After having successfully synthesized the monolayer-protected gold nanoclusters (Au–MPCs), the samples were further purified by several cycles of re-solvation in water and re-precipitation by adding methanol. The as-prepared clusters were then characterized and studied by UV-vis spectroscopy, transmission electron microscopy (TEM), circular dichroism spectroscopy (CD), thermogravimetric analysis (TGA), and photoluminescence spectroscopy.

3.1 Size and Chemical Composition of Synthesized Gold Clusters

One of the most effective ways to obtain the ratio between organic fraction and the metal content is thermogravimetry. With this technique the metal-to-ligand ratio (M/L) and, hence, the average chemical formula of the MPCs can be derived. Penicillamine that was used as protecting ligands decomposes when heating up to 231°C in a single step (Fig. 1c and d). Fig. 1 shows the thermograms of all cluster samples and a common trend is observed: All clusters are found to be hygroscopic, which is indicated by the onset of the mass loss already at 40°C temperature.

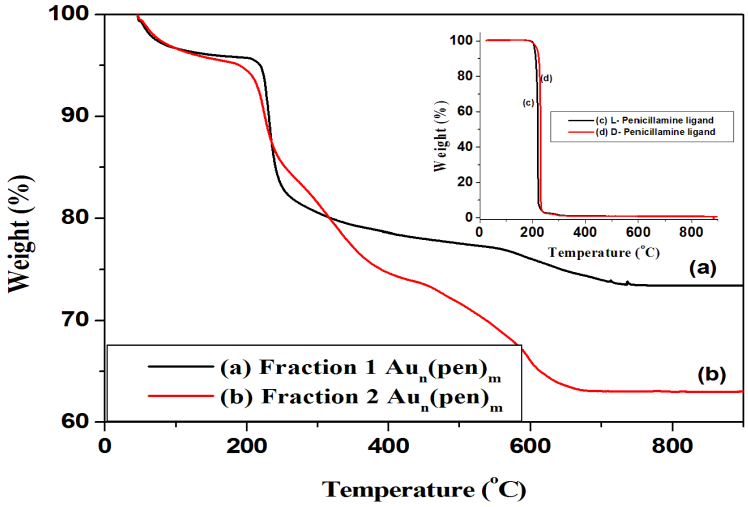

Figure 1. Thermogravimetric analysis of fraction 1 (**curve a**) and fraction 2 (**curve b**) gold clusters. Both fractions of gold clusters consist of same ligand but differ in cluster size. All curves show an onset already at 40 °C, which is due to the removal of water molecules, showing that the clusters are hygroscopic. Furthermore, several steps can be found, which are due to the decomposition of the organic molecules. For the two samples, the destruction of the organic compound is completed before 900 °C. Therefore, it can be concluded that the residual mass of the clusters samples consists of gold atoms only and, hence, the average molecular formula of the clusters can be calculated. Curve c and d show the thermogravimetric analysis (TGA) of the bare penicillamine ligands. The ligands decompose in one step at 231°C.

A mass loss at these low temperatures is attributed to the removal of adsorbed water molecules rather than to a decomposition of the ligand, since the pure ligand does not show any mass loss up to 200°C [2,24]. With the exception of the removal of water molecules, the other steps of the TGA curve correspond to the decomposition of the ligand protecting clusters. In the measurements of all species the decomposition of the ligand is completed before 900°C and the residue consists of metal atoms, only (Table 1). By the comparison of the TGA curves of clusters of different core sizes it is found that larger clusters show a higher metal-to-ligand ratio than smaller ones (Table 1). This behaviour is observed because the numbers of atoms inside the metal core becomes larger with respect to the numbers of surface atoms of the particle. From

the relative weight of the residue with respect to the total weight loss of organic molecules, the average ligand-to-metal ratio can be calculated and thus the average molecular formula of the clusters can be derived [2,24,25]. The results together with all the thermogravimetric data are shown in Table 1. The percentage of gold part in fraction 1 is 73.44 % and fraction 2 is 63.02 % (Table 1), the calculated weight of gold part in $Au_{25}(pen)_{18}$ is 64.7 %, therefore, the synthesized fraction 2 expects to be size selected clusters (Au_{25}) protected by penicillamine.

Table 1. Results of the thermogravimetric analysis of gold clusters.

Sample	Thermal degradation step	t_{onset} (°C)	t_{end} (°C)	Weight loss (%)	Weight (%) at 900°C	M/S ratio	Molecular formula
First fraction $Au_n(Pen)_m$	I	46	187	4.38	73.44	1:0.39	~$Au_{3n}L_n$
	II	187	320	16.63			
	III	320	800	5.55			
Second fraction $Au_n(Pen)_m$	I	46	185	5.05	63.02	1:0.66	$Au_{3n}L_{2n}$
	II	185	273	10.98			
	III	273	433	9.92			
	IV	433	750	11.03			

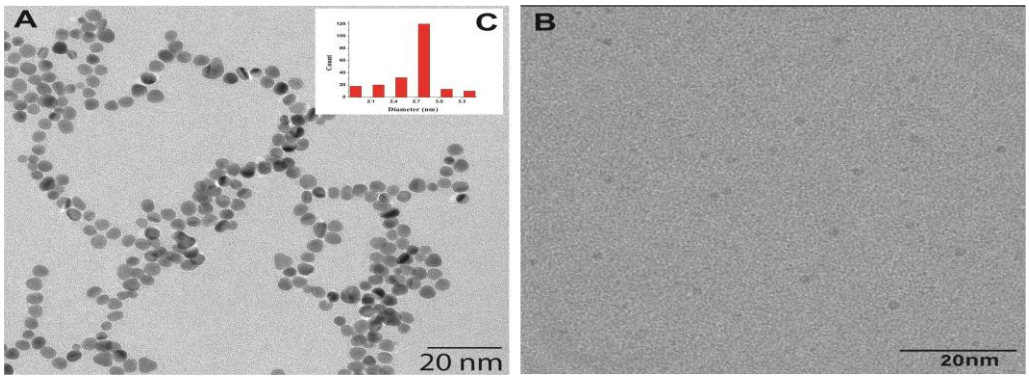

Figure 2. Transmission electron microscope (TEM) images of first fraction of $Au_n(L\text{-pen})_m$ nanoclusters with an average size of 2.66 nm **(A)** and the second fraction of $Au_n(L\text{-pen})_m$ nanoclusters (**B**). In the image of the second fraction the clusters look very uniform and have a size of around 1 nm. (**C**) Size distribution of first fraction $Au_n(L\text{-pen})_m$ nanoclusters. $Au_n(L\text{-pen})_m$ nanoclusters consist of an average size of 2.66 nm (213 particles were used to obtain this average size) and a very smooth Gaussian distribution over the cluster size is found.

For the determination of the average size and the size distribution of the metal clusters transmission electron microscopy (TEM) is one of the most often used techniques [2,24,25]. Conventional TEM is particularly powerful when the particle size is larger than 1 nm, because large scattering cross sections of the metal atoms result in a strong contrast in the TEM image. For smaller clusters (below 1 nm in diameter), however, the contrast becomes very weak and hence such small particles may not be detected and counted [2,4]. In addition, another drawback of TEM is that the cluster samples are casted onto a surface (in this work on carbon-coated copper grids). As a consequence, migration and coalescence of the particles may occur. In the case of monolayer protected clusters coalescence may be ruled out, due to the protection by ligands.

Fig. 2 shows TEM images of the two fractions of gold clusters protected by L-penicillamine (L-pen) ligand. In general, individual spherical nanoparticles can be seen for all the samples. The particles sizes of second traction are very homogeneous in size and of about 1 nm (Fig. 2B), clusters of the first fraction have an average size of 2.66 nm (Fig. 2A). This is a clear indication that particles with a very narrow size distribution (Fig. 2C), can be obtained with this synthesis method. Furthermore, as expected, the particle sizes of gold clusters protected by different enantiomers of the ligand do not change.

3.2 Optical Properties of the Synthesized Gold Clusters.

Plasmonic metal nanoparticles (Au and Ag) have a great potential for chemical and biological sensor applications, due to their sensitive spectral response to the local environment of the nanoparticles surface and the ease of monitoring the light signal due to their strong scattering or absorption [26]. In addition, the UV-vis spectra are very sensitive to changes in the metal core of the particles, in particular for clusters comprising of only a few tens of atoms. The optical response can thus be used to estimate and monitor the size of the particles.

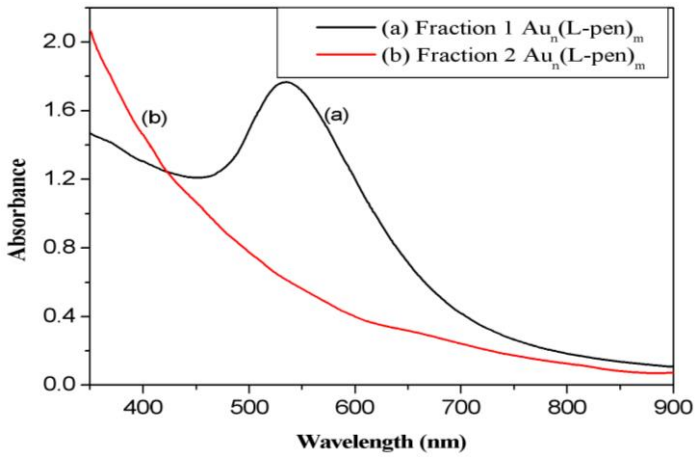

Figure 3. UV−vis absorption spectra of Au nanoparticles $Au_n(L\text{-pen})_m$ of different sizes. Fraction 1 consists of particles of an average size of 2.66 nm and shows a well-defined surface plasmon band at 534 nm a (curve a). Particles of fraction 2 are much smaller (around 1 nm) and give a multiband absorption spectrum with a distinct a peak at around 670 nm and another two shoulders at 400, 450 nm (curve b). These absorption bands very well resemble the spectroscopic fingerprints of gold nanoclusters consisting of a metallic core of exactly 25 Au atoms [2,4].

2 nm regime silver and gold monolayer-protected clusters in general exhibit a broad plasmon resonance peak at around 450 nm and 550 nm in the visible region, respectively [2,25]. It was shown previously that for particles of this size the transition can be modelled by Mie theory in combination with the Drude model, which clearly demonstrates that such peaks originate from plasmonic transitions [24].

In accordance to such observations, fraction 1 from gold clusters protected by L-penicillamine (L-pen) consists of an average particle size of around 2.66 nm and, consequently, the UV−vis spectrum shows a surface plasmon absorption band at 534 nm (curve a in Fig. 3). Due to their smaller size of about 1 nm, clusters of the second fraction (curve b in Fig. 3), however, exhibit a broad absorption spectrum with one weak band at around 670 nm and another two small shoulders at 400 and 450 nm (curve b in Fig. 3). These absorption bands resemble very well the spectroscopic fingerprints of Au_{25} nanoclusters [27,28], which are usually found for monodisperse clusters consisting of a metal core of exactly 25 atoms, such as $Au_{25}(SG)_{18}$ [4] and $Au_{25}(SR)_{18}$ (SR = SCH_2CH_2Ph, $SC_{12}H_{25}$, and SC_6H_{13}) [29]. Therefore, the UV-vis spectrum of fraction 2 of the $Au_n(L\text{-pen})_m$ clusters again confirms the observations obtained from TEM of a very narrow particle size distribution and furthermore suggests that the clusters are monodisperse and consist of core sizes of Au_{25}.

Note that the spectra of all samples are the same, which shows the expected behaviour, namely that different enantiomers of the same ligand do neither effect the peak position nor its broadness.

3.3 Chirality of the Gold Monolayer-Protected Clusters (Au-MPCs).

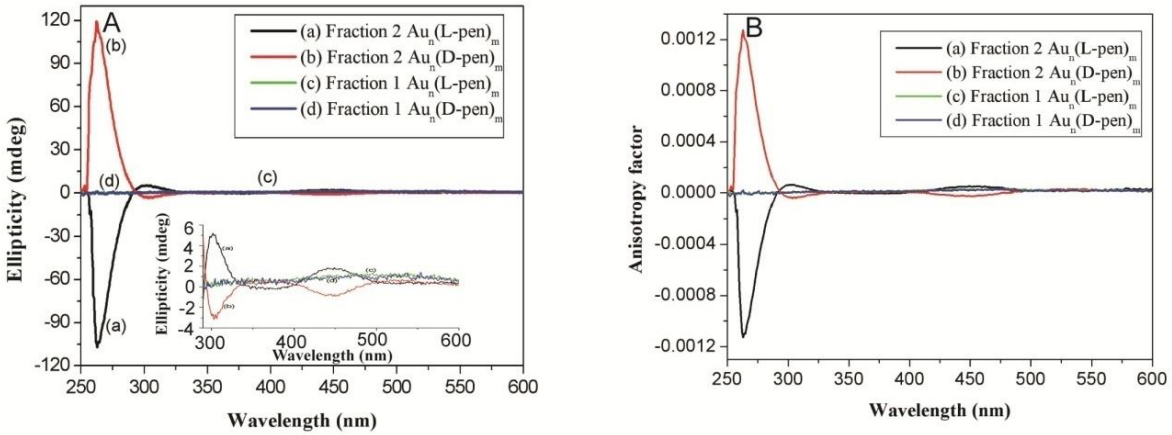

Figure 4. CD spectra and anisotropy factors of second fraction gold clusters $Au_n(L\text{-pen})_m$ (curve a) and $Au_n(D\text{-pen})_m$ (curve b) and the first fraction of $Au_n(L\text{-pen})_m$ (curve c) and $Au_n(D\text{-pen})_m$ (curve d) nanoclusters. The second fraction of gold nanoclusters shows mirror images circular dichroism signals in the range from 250 to 600 nm. The first fraction from

gold clusters, however, does not give any CD peaks **(A)**. **(B)** Corresponding anisotropy factors for all gold cluster samples calculated out of the CD and absorption spectra. Large factors for a metal cluster sample of up to $1.3x10^{-3}$ are found. (Note that curve c in **(B)** can hardly be seen, since it is almost entirely overlaid by curve d.)

The exploration of the origin of chirality in monolayer protected clusters protected by chiral ligands has been a very active research field in the last few decades [30,31]. The chirality of the clusters can be studied by CD spectroscopy. While large particles (>2 nm) usually give small chiroptical peaks, the bands of smaller clusters are much pronounced [2,24,32]. This observation of a decreasing optical activity with increasing particle size, can simply be explained by the increased configurational space for larger particles (larger number of gold atoms and ligands) and thus an increased probability of multiple energy minima on the potential energy surface. An increasing number of conformers lead to a decreased optical activity as positive and negative bands of different conformers average out [33].

The CD spectra of particles covered with the two penicillamine enantiomers (L-pen and D-pen) show a mirror image relationship – a typical behavior for enantiomers. The CD spectra of the clusters protected by the two different enantiomeric forms of the ligand give perfect mirror images with several signals in the region from 250 nm to 600 nm (Fig. 4A). In contrast to the spectra of the cluster that even exhibit bands in the visual region, the bare ligand molecule only show significant CD signals below 250 nm [18]. While bands after 250 nm in the spectra of the clusters may therefore be interpreted as clearly indicate metal-based origins.

The two fractions of gold clusters show a completely different behaviour. As expected, larger cluster of fraction 1 (average size of about 2.66 nm) do not give significant CD signals above 250 nm [2,18]. Smaller clusters of about 1 nm, however, exhibit three well-resolved transitions (264, 305, 370 and 447 nm). The spectra are much pronounced than previously reported ones of Yao et al. [18], who have obtained clusters of different sizes by separating a polydisperse mixture with gel electrophoresis. In all cases, peaks are found in a similar wavelength range, with the occurrence of metal-based bands above 300 nm. However, we again assign the differences in the spectra (different band positions, different number of bands and different spectral shapes, which cannot be explained by a superposition of the spectra of differently sized clusters) to different cluster morphologies or to different chemical compositions.

For a better comparison, which is not dependent on the sample concentration, usually the anisotropy factor is calculated. Anisotropy factors (g) are defined as the difference in absorption of left- and right-handed circularly polarized light (ΔA) divided by the absorption of the racemate (A).

$$g = \Delta A/A \qquad \text{(Eq.1)}$$

The factor can be calculated from the measured ellipticity (θ) and the absorption spectrum by using the following equation:

$$g = \theta[\text{mdeg}]/(32980 \times A) \qquad \text{(Eq. 2)}$$

The result over the entire spectral range can be seen in the Fig. 4B. It is found that the anisotropy factors are quite large for a cluster sample. In particular, for the small gold clusters of about 1 nm the anisotropies range up to $1.3x10^{-3}$. Notably, this value is not only one order of magnitude higher than that for the same gold clusters obtained via separation with gel electrophoresis [18], but even is one of the largest for gold clusters, in general. So far very high anisotropy values have for example been reported for gold nanoclusters protected with 1,1′-binaphthyl-2,2′-dithiol chiral ligand (4×10^{-3}) [34] and intrinsically chiral $Au_{38}(SCH_2CH_2Ph)_{24}$ ($1x10^{-3}$) [23].

3.4 Photoluminescence of Monolayer-Protected Clusters (Au-MPCs).

The exact mechanism of the photoluminescence (PL) of monolayer protected noble metal cluster is still under debate. Due to the non-fluorescent properties of the ligand (in this work penicillamine), the fluorescence must originate from the metal core. The ligand, however, can strongly influence PL and, in particular, largely increase its intensity as indicated by the investigation of several Au_{25} clusters [29]. In general, among ligand protected clusters, gold clusters have been studied the most widely by PL. Already in 1998 an influence of size of spherical gold clusters on PL was reported [35]. With liquid chromatography two fractions were separated; one of small clusters (smaller than 5 or 2.5 nm), which exhibited very strong PL but gave no well-resolved plasmon peak and another one with clusters of about 15 nm, where a distinct plasmon peak but no PL was observed [35].

A similar behaviour is found for clusters of $Au_n(pen)_m$. While the first fraction of clusters with an average size of about 2.66 nm give a strong and good resolved plasmon peak in their absorbance spectra (Fig. 3a), no PL is detected (Fig. 5). The quenching of the fluorescence accompanied by the appearance of a pronounced plasmon transition for larger clusters can also be found for other gold systems (as e.g. for the Au-particle growth on SiO_2) [36]. Usually, big particles only show fluorescence if they consist of multiple grains, otherwise the density of states of the clusters is too high for the clusters being luminescent [37,38].

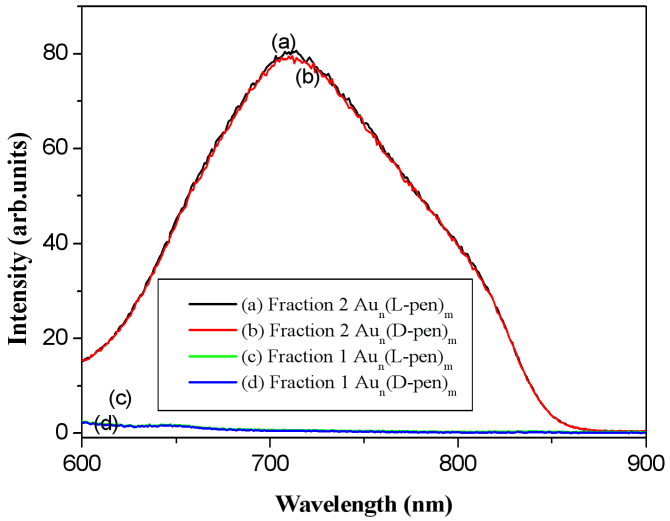

Figure 5. Photoemission spectra of the two fractions of gold clusters protected by L-penicillamine (L-pen) and D-penicillamine (D-pen) were measured. Gold clusters of the second fractions of gold clusters exhibit a broad emission maximum at 715 nm, which is independent of the enantiomeric form of the protective ligand. Clusters of the first fraction, however, do not show any emission maximum at all. (Note that curve c and d in are almost identical and, thus, the first one can hardly be seen).

On the other hand, $Au_n(pen)_m$ clusters of fraction 2 of about 1 nm in size exhibit a broad band at 715 nm in the PL spectrum after excitation at 450 nm (Fig. 5). This result is in very good agreement with the spectra of Au_{25} cores protected by different ligands [29], which further indicates that clusters of fraction 2 may have Au_{25} cores. Furthermore, the asymmetry of the band indicates that possibly two luminescence pathways contribute to the spectra. It was found [39] that small gold clusters are excited from the d-band into the sp-band and then radiatively decay via an intraband transition into lower levels of the sp-band or in a second path back to the levels of the d-band. While the first path gives rise to a low energy PL band, the latter one results in a transition of higher photon energies [39]. Note that in a molecular picture the transitions are interpreted as fluorescence and phosphorescence, with the latter resulting from the emission of photons with lower energies [39]. Devadas et. al. used the structure of Au_{25} clusters to supply a further interpretation of the two processes [40]. The first process resulting in the PL of photon with higher energies (in their case 500 nm) was assigned to a recombination process almost entirely in the Au_{13} core with just little perturbation from the surface ligands. For the second process, however, resulting in the band in the NIR region (i.e. around 700 nm), a decay mechanism via the semi ring states of the outer part of the metal core was suggested [40].

4 Conclusions

In this work we present the synthesis, the characterization and the optical properties of gold nanoparticles protected by two enantiomers penicillamine and the racemic mixture. Methanol induced precipitation method allows for the separation of two fractions with different particle sizes. The advantages to this method produces size selected clusters with high yield products and by easy way. The first fraction consists of clusters of 2.66 nm, as determined by TEM analysis. Particles of this fraction exhibit a typical plasmon transition in their absorption spectrum, but neither gives any significant CD signal above 250 nm nor shows any photoluminescence properties. Clusters of the second fraction, however, are about 1 nm in diameter, as determined by TEM images. In their absorption spectra a multi-band absorbance rather than a well-resolved plasmon peak is observed, which strongly resembles the typical spectra of Au_{25} cores. In addition, these clusters show several transitions in their CD spectra with high asymmetry factor in comparison to the spectra of most other ligand protected clusters. Furthermore, a broad peak with a maximum around 715 nm is observed in the photoluminescence of these clusters, which is again in good agreement to the spectra of clusters with Au_{25} cores, which are protected by other ligands. The asymmetry of the peak in the spectrum further points to two involved recombination pathways. From TGA, UV-vis and PL analysis we can expect the synthesized second fraction is $Au_{25}(pen)_{18}$.

While new insights on the optical properties of Au clusters protected by penicillamine are obtained in this work, the synthetic route chosen results in high cluster yield in comparison to methods using chromatography for size separation. This significantly higher yield of sample has allowed for a more thorough and better characterization of the samples and will enable further studies on the applicability of these systems as sensors or asymmetric catalysts [41-44].

Acknowledgements

This work is supported by Assiut University, Egypt. I kindly acknowledge Prof. Dr. U. Heiz and Dr. M. Tschurl for carrying out circular dichroism measurement and for helpful discussions in Technical University of Munich (TUM).

References

[1] P. D. Jadzinsky, G. Calero, C. J. Ackerson, D. A. Bushnell, R. D. Kornberg, Science, **318**, 430 (2007)

[2] M. Farrag, M.Tschurl, U. Heiz, Chem. Mater., **25**, 862 (2013).

[3] M. Farrag, M. Tschurl, A. Dass, U. Heiz, Phys. Chem. Chem. Phys., **15**, 12539 (2013).

[4] B. Z. Wu, J. Chen, R. Jin, Adv. Funct. Mater., **21**, 177 (2011).

[5] M. Brust, M. Walker, D. Bethell, D. J. Schiffrin, R. Whyman, J. Chem. Soc. Chem. Commun., **801**. (1994).

[6] W. W. Weare, S. M. Reed, M. G. Warner, J. E. Hutchison, J. Am. Chem. Soc., **122**, 12890 (2000).

[7] Y. Shichibu, K. Suzuki, K. Konishi, Nanoscale, **4**, 4125 (2012).

[8] S. Gomez, K. Philippot, V. Colliere, B. Chaudret, F. Senocq, P. Lecante, Chem. Commun., 1945 (2000).

[9] A. Kumar, S. Mandal, P. R. Selvakannan, R. Pasricha, A. B. Mandale , M. Sastry, Langmuir, **19**, 6277 (2003).

[10] M. Zhu, C. M. Aikens, F. J. Hollander, G. C. Schatz, R. Jin, J. Am. Chem. Soc., **130**, 5883 (2008).

[11] J. Akola, M. Walter, R. L. Whetten, H. Häkkinen, H. Grönbeck, J. Am. Chem. Soc. **130**, 3756 (2008).

[12] M. Zhu, C. M. Aikens, M. P. Hendrich, R. Gupta, H. Qian, G. C. Schatz, R. Jin, J. Am. Chem. Soc. **131**, 2490 (2009).

[13] T. G. Schaaff, R. L. Whetten, J. Phys. Chem. B, **104**, 2630–2641 (2000).

[14] C. Gautier, R. Taras, S. Gladial, T. Burgi, Chirality, **20**, 486–493 (2008).

[15] C. Gautier, T. Burgi, Chem. Commun., 5393–5395 (2005).

[16] C. Gautier, T. Burgi, J. Phys. Chem. C, **114**, 15897–15902 (2010).

[17] H. Qian, W. T. Eckenhoff, Y. Zhu, T. Pintauer, R. Jin, J. Am. Chem. Soc., **132**, 8280–8281 (2010).

[18] H. Yao, K. Miki, N. Nishida, A. Sasaki, K. Kimura, J. Am. Chem. Soc., **127**, 15536–15543 (2005).

[19] S. Knoppe, A. C. Dharmaratne, E. Schreiner, A. Dass, T. Bürgi, J. Am. Chem. Soc., **132**, 16783–16789 (2010).

[20] V. R. Jupally, R. Kota, E. Van Dornshuld, D. L. Mattern, G. S. Tschumper, D. Jiang, A. Dass, J. Am. Chem. Soc., **133**, 20258–20266 (2011**)**.

[21] M. Zhu, H. Qian, X. Meng, S. Jin, Z. Wu, R. Jin, Nano Lett., **11**, 3963–3969 (2011).

[22] M. W. Heaven, A. Dass, P. S. White, K. M. Holt, R. W. Murray, J. Am. Chem. Soc., **130**, 3754–3755 (2008).

[23] I. Dolamic1, S. Knoppe, A. Dass, T. Bürgi, Nat. Commun., **3**, 798. (2012).

[24] M. Farrag, M. Thämer, M. Tschurl, T. Bürgi, U. Heiz, J. Phys. Chem. C, **116**, 8034. (2012).

[25] A. Taleb, C. Petit, M. P. Pileni, Chem. Mater. **9**, 950 (1997).

[26] R. Jin, Nanoscale, **2**, 343 (2010).

[27] M. Zhu, C. M. Aikens, F. J. Hollander, G. C. Schatz, R. Jin, J. Am. Chem. Soc., **130**, 5883 (2008).

[28] Z. Wu, J. Suhan, R. Jin, J. Mater. Chem., **19**, 622 (2009).

[29] Z. Wu, R. Jin, Nano Lett., **10**, 2568 (2010).

[30] I. L. Garzón, J. A. Reyes-Nava, J. I. Rodríguez-Hernández, I. Sigal, M. R. Beltrán, K. Michaelian, Phys. Rev. B, **66**, 073403 (2002).

[31] I. L. Garzón, M. R. Beltrán, G. González, I. Gutíerrez-González, K. Michaelian, J. A. Reyes-Nava and J. I. Rodríguez-Hernández, Eur. Phys. J. D, **24**, 105 (2003).

[32] T. G. Schaaff, R. L. Whetten, J. Phys. Chem. B, **104**, 2630 (2000).

[33] C. Gautier, T. Bürgi, J. Am. Chem. Soc., **128**, 11079 (2006).

[34] C. Gautier, R. Taras, S. Gladiali, T. Bürgi, Chirality, **20**, 486 (2008).

[35] J. P. Wilcoxon, J. E. Martin, F. Parsapour, B. Wiedenman, D. F. Kelley, J. Chem. Phys., **108**, 9137 (1998).

[36] M. Eichelbaum, K. Rademann, A. Hoell, D. M. Tatchev, W. Weigel, R. Stößer, G. Pacchioni, Nanotechnology, **19**, 135701 (2008).

[37] J. Zheng, C. Zhou, M. Yu, J. Liu, Nanoscale, **4**, 4073 (2012).

[38] C. Zhou, J. Yu, Y. Qin, J. Zheng, Nanoscale, **4**, 4228 (2012).

[39] S. Link, A. Beeby, S. Fitz Gerald, M. A. El-Sayed, T. G. Schaaff, R. L. Whetten J. Phys. Chem. B, **106**, 3410 (2002).

[40] M. S. Devadas, J. Kim, E. Sinn, D. Lee, T. Goodson, G. Ramakrishna, J. Phys. Chem. C, **114**, 22417 (2010).

[41] M. Farrag, J. Mol. Catal. A: Chem., **41**, 67-76 (2016).

[42] M. Farrag, J. Photochem. Photobiol. A: Chem., **318**, 42–50 (2016).

[43] M. Farrag, Micropor. Mesopor. Mat., **232**, 248-255 (2016).

[44] M. Farrag, Mater. Chem. Phys., **180**, 349-356 (2016).